



**HAL**  
open science

## Boron-induced phase transformation of ternary cerium boron silicides

Volodymyr Babizhetskyy, Reinhard K. Kremer, Régis Jardin, Régis Gautier, Bruno Fontaine, Jean-François Halet

► **To cite this version:**

Volodymyr Babizhetskyy, Reinhard K. Kremer, Régis Jardin, Régis Gautier, Bruno Fontaine, et al.. Boron-induced phase transformation of ternary cerium boron silicides. *Solid State Sciences*, 2023, *Solid State Sciences*, pp.107378. 10.1016/j.solidstatesciences.2023.107378 . hal-04303421

**HAL Id: hal-04303421**

**<https://hal.science/hal-04303421>**

Submitted on 29 Nov 2023

**HAL** is a multi-disciplinary open access archive for the deposit and dissemination of scientific research documents, whether they are published or not. The documents may come from teaching and research institutions in France or abroad, or from public or private research centers.

L'archive ouverte pluridisciplinaire **HAL**, est destinée au dépôt et à la diffusion de documents scientifiques de niveau recherche, publiés ou non, émanant des établissements d'enseignement et de recherche français ou étrangers, des laboratoires publics ou privés.

# Boron-induced phase transformation of ternary cerium boron silicides

Volodymyr Babizhetskyy<sup>a,\*</sup>, Reinhard K. Kremer<sup>b</sup>, Régis Jardin<sup>c,d</sup>, Régis Gautier<sup>c</sup>, Bruno Fontaine<sup>c,e,\*</sup>, Jean-François Halet<sup>c,f,\*</sup>

<sup>a</sup> *Department of Inorganic Chemistry, Ivan Franko National University of Lviv, Kyryla i Mefodiya Str. 6, UA-79005 Lviv, Ukraine*

<sup>b</sup> *Max-Planck-Institut für Festkörperforschung, Heisenbergstrasse 1, Postfach 800665, D-70569 Stuttgart, Germany*

<sup>c</sup> *Univ Rennes, CNRS, École Nationale Supérieure de Chimie de Rennes, Institut des Sciences Chimiques de Rennes (ISCR) – UMR 6226, F-35000 Rennes, France*

<sup>d</sup> *Bruker AXS GmbH, Östliche Rheinbrückenstraße 49, D-76187 Karlsruhe, Germany*

<sup>e</sup> *Saint-Cyr Coëtquidan Military Academy (CReC), F-56380 Guer, France*

<sup>f</sup> *CNRS – Saint-Gobain – NIMS, IRL 3629, Laboratory for Innovative Key Materials and Structures (LINK), National Institute for Materials Science (NIMS), Tsukuba, 305-0044, Japan*

*Dedicated to a long-time friend, Professor André Perrin on the occasion of his 80th birthday.*

## ABSTRACT

Samples of the alloys  $\text{CeSi}_{2-x}\text{B}_x$  ( $x = 0, 0.1, 0.2, 0.4, \text{ and } 0.5$ ) were prepared and their crystal structures, electrical and magnetic properties were determined. Depending on the amount of boron,  $x$ , the phases  $\text{CeSi}_{2-x}\text{B}_x$  crystallize in the  $\alpha\text{-ThSi}_2$  structure type ( $x = 0, 0.1$ ), or in the  $\alpha\text{-GdSi}_2$  structure type ( $x = 0.2, 0.4$ ). Interestingly, as determined by means of X-ray single crystal diffraction crystallizes,  $\text{CeSi}_{1.5}\text{B}_{0.5}$  crystallizes in the  $\text{AlB}_2$  structure type (space group  $P6/mmm$ ,  $a = 3.9922(2)$ ,  $c = 4.3053(4)$  Å, 191 reflections with  $I_o \geq 2\sigma(I_o)$ ,  $R_1 = 0.019$ ,  $wR_2 = 0.042$ ). Measurements of the electrical and magnetic properties indicate that phases  $\text{CeSi}_{2-x}\text{B}_x$  ( $x = 0, 0.1, 0.2, 0.4, 0.5$ ) are metallic in character and that phases with B substitution  $x \geq 0.2$  exhibit correlated magnetic behavior, typically below  $\sim 15$  K. Density functional theory calculations were performed to elucidate the change of electronic and physical properties upon boron substitution.

*Keywords:* Crystal structure; Density functional calculations; Electronic structure; Magnetism; Rare-earth metal silicide boride; Silicide boride

---

\* Corresponding authors.

*E-mail addresses:* [volodymyr.babizhetskyy@lnu.edu.ua](mailto:volodymyr.babizhetskyy@lnu.edu.ua) (V. Babizhetskyy);

[bruno.fontaine@ensc-rennes.fr](mailto:bruno.fontaine@ensc-rennes.fr) (B. Fontaine); [Jean-Francois.Halet@univ-rennes.fr](mailto:Jean-Francois.Halet@univ-rennes.fr) (J.-F. Halet)

## 1. Introduction

A first systematic study of the ternary phase diagrams of the  $RE$ -Si-B ( $RE = Y, La, Ce, Er$ ) phases was reported by Kuz'ma and co-workers some time ago [1–3]. At that time, the existence of ternary phases was not evidenced, with the exception of narrow homogeneity ranges of some specific binary compositions. More recently, in the progress of our ongoing investigation of structural and physical properties of ternary  $RE$ -Si-B phases ( $RE =$  rare earth metals), different preparation techniques were explored (sealed silica tubes, arc melting, high frequency furnace, and tin flux synthesis), resulting in the synthesis and characterization of several new binary and ternary rare-earth metal boron silicides [4–6]. For example, using arc melting techniques on the isothermal sections of the ternary systems  $RE$ -Si-B ( $RE = Y, Nd, Gd, Dy, Ho, Er$ ) at 1270 K [7–9] we found that, except for Nd, a few new ternary phases could be synthesized, namely the stoichiometric compound  $RE_5Si_2B_8$  ( $Gd_5Si_2B_8$  structure type) [10, 11], the boron-inserted ‘Nowotny phase’  $RE_5Si_3B_x$  ( $Mn_5Si_3$ -type structure) [12], and the solid solution  $REB_{2-x}Si_x$  ( $AlB_2$ -type structure) [1]. For the Nd-Si-B system, only  $Nd_5Si_3B_x$  ( $Mn_5Si_3$ -type structure) could be ascertained [8]. Using flux techniques [13] with tin as the metal flux a novel series of binary silicides of composition  $RESi_{1.7}$  ( $RE = Dy, Ho$ ) [14] were obtained, as well as new layered ternary boride silicides in the silicon-rich part of the  $RE$ -Si-B phase diagram, namely  $RE_8Si_{17}B_3$  ( $RE = Ho, Er$ ) [1],  $RE_9Si_{15-x}B_3$  ( $RE = Tb, Yb$ ) [2] and  $Er_3Si_{5-x}B$  ( $x = 1.17$ ) [15]. It turned out that the insertion of boron atoms into the silicon slabs in these new ternary structures generates ordered commensurate arrangements in the  $c$  direction, which can be derived from the  $AlB_2$  structure type [15].

In 2002, Bulanova *et al.* investigated and constructed the phase diagram of the Ce-Si binary system [16]. In the region of ~66 at. % Si they identified two cerium disilicides namely  $CeSi_{2-a1}$  ( $0.43 > a1 > 0.3$ ) crystallizing with the  $\alpha$ - $GdSi_2$  structure type (space group (SG)  $Imma$ ) and  $CeSi_{2-a2}$  ( $0.3 > a2 > 0$ ) crystallizing with the  $\alpha$ - $ThSi_2$  structure type (SG  $I4_1/amd$ ). According to these authors, the phases with the  $\alpha$ - $GdSi_2$  and the  $\alpha$ - $ThSi_2$  structures seem to correspond to

individual compounds rather than polymorphous modifications of the same compound  $\text{CeSi}_{2-a}$ . This statement was made on the basis of the absence of thermal effects in the range  $\text{CeSi} + \text{CeSi}_{2-a1}$  at temperatures lower than the solidus, and also by analogy with the La–Si and Pr–Si systems [16]. The boundaries of the two-phase field  $\text{CeSi}_{2-a1}$  and  $\text{CeSi}_{2-a2}$  are located between 62.6 and 64.1 at % Si and they shift towards Si-poorer compositions when the temperature decreases.  $\text{CeSi}_{2-a1}$  in the  $\alpha\text{-GdSi}_2$  structure type exists between 62 and 65 at. % Si whereas  $\text{CeSi}_{2-a2}$  ( $\alpha\text{-ThSi}_2$  structure type) covers the range between 65.0 and 66.7 at. % Si [17]. Later, an incommensurately modulated structure of  $\text{CeSi}_{2-x}$  ( $x = 1.82$ ) with reduced monoclinic symmetry was reported by Leisegang *et al.* [18]. Modulated crystals and crystals without satellite reflections were found simultaneously in the same macroscopic sample showing composition changes of about 4 % ( $1.87 < x < 1.91$ ) [18].

It turns out that the compounds  $\text{CeSi}_{2-a1}$  and  $\text{CeSi}_{2-a2}$  or more generally  $\text{CeSi}_{2-x}$ , exhibit a strong variation of physical properties when changing the composition from  $a1$  to  $a2$  ( $x$ ). Long range ferromagnetic ordering of the Ce atoms due to a Ruderman-Kittel-Kasuya-Yosida (RKKY) interaction was observed at temperatures  $T_m \approx 12$  to 1 K and for compositions with  $x$  varying from 0.40 to 0.18. For values  $x = 0.40$  to 0.18, Kondo behavior (Kondo temperature  $T_K = 2 - 22$  K) leads to the absence of magnetic ordering. These properties arise from an exchange interaction between the conduction electrons and the Ce  $4f$  electrons [19-23].

Due to the wide homogeneity region of  $x = 0 - 0.4$ ,  $\text{CeSi}_{2-x}$  is indeed an interesting system to study in order to elucidate the influence of the non-magnetic Si deficiency on the structural and physical properties. Additionally, we may wonder if insertion of a third element such as boron, for example, would also modify the structural arrangement and consequently alter in some ways the physical properties.

Here we report on a detailed investigation of structural, electrical and magnetic properties of samples with composition  $\text{CeSi}_{2-x}\text{B}_x$  ( $x = 0, 0.1, 0.2, 0.4, \text{ and } 0.5$ ) prepared by arc melting techniques. In particular, the novel ternary boride silicide  $\text{CeSi}_{1.5}\text{B}_{0.5}$  was synthesized and

characterized. The structure determination from single-crystal X-ray diffraction data indicates that  $\text{CeSi}_{1.5}\text{B}_{0.5}$  adopts the  $\text{AlB}_2$  type structure [15, 24] with a mixed Si/B site occupation. Moreover, the presence or absence of inserted boron atoms in  $\text{CeSi}_{2-x}\text{B}_x$  is discussed on the basis of difference Fourier syntheses, structural analysis, electrical and magnetic behavior and density functional theory (DFT) calculations.

## 2. Experimental section

### 2.1. Synthesis

The samples with compositions  $\text{CeSi}_{2-x}\text{B}_x$  ( $x = 0, 0.1, 0.2, 0.4, \text{ and } 0.5$ ) were prepared from commercially available elements: Ce-sublimed bulk pieces, 99.99 at. % (Alfa Aesar, Johnson Matthey Company), powders of elemental silicon and boron (Strem Chemicals, purity > 99.99 at. %). Cerium metal was filed to coarse powders with beryllium bronze files (Dönges GmbH, Germany). Mixtures of the components were compacted in stainless steel dies and the resulting pellets of  $\sim 1$  g were arc-melted under purified argon atmosphere on a water-cooled copper hearth, turned over and re-melted typically three times to improve homogeneity. The sample-buttons were then wrapped in a molybdenum foil enclosed in an evacuated silica tube, annealed at 1070 K for one month, and then the tube was quenched in cold water.

### 2.2. Diffraction and sample characterization

An initial metallographic inspection and complementary qualitative and quantitative phase analysis, energy dispersive X-ray spectroscopy (EDX) was employed. The samples were embedded in Wood's metal (melting point of 75 °C, Fluka Chemie). The embedded samples were polished on a nylon cloth using diamond paste with grain sizes 1–5  $\mu\text{m}$ . Quantitative and qualitative composition analyses of the polished samples were performed by EDX on a TESCAN VEGA 3 LMU scanning electron microscope with an Oxford Instruments Aztec ONE detector X-Max<sup>N</sup>20. For the chemical microprobe, the polishing procedure had to be performed or

repeated just before the measurements. This method was further used to determine the Ce:Si ratios of the synthesized specimen (standard deviations estimated less than 1 at.%). Unfortunately, no boron content could be determined by a quantitative microanalysis. The surface of the phases  $\text{CeSi}_{2-x}\text{B}_x$  ( $x = 0, 0.1, 0.2, 0.4, \text{ and } 0.5$ ) appears to be quite stable in air.

Powder X-ray diffraction (PXRD) patterns of  $\text{CeSi}_{2-x}\text{B}_x$  ( $x = 0, 0.1, 0.2, 0.4, \text{ and } 0.5$ ) were collected on a STOE STADI P powder diffractometer with monochromated  $\text{Mo-K}\alpha_1$  radiation ( $3^\circ \leq 2\theta \leq 60^\circ$ , step size  $0.1^\circ$ , measurement time per step: 120 s) to check the homogeneity of the samples. The lattice parameters and the atomic positions the PXRD were fitted by a Rietveld-type profile refinement using the WinCSD program package [25]. The PXRD pattern of the alloy with nominal compositions  $\text{CeSi}_{2-x}\text{B}_x$  ( $x = 0, 0.1, 0.2, 0.4, \text{ and } 0.5$ ) confirmed the presence of three phases: the  $\alpha\text{-GdSi}_2$ ,  $\alpha\text{-ThSi}_2$  and  $\text{AlB}_2$  structure types, respectively (details see Table 1).

**Table 1**

Crystal structure parameters from XRD powder data for  $\text{CeSi}_{2-x}\text{B}_x$  ( $x = 0, 0.1, 0.2, 0.4, 0.5$ ).

Composition	Space group	Structure type	Cell parameters (Å)			Full profile refinement residuals $R_B, R_p$
			<i>a</i>	<i>b</i>	<i>c</i>	
$\text{CeSi}_2$	<i>I4<sub>1</sub>/amd</i>	$\alpha\text{-ThSi}_2$	4.1931(2)		13.9132(7)	0.060, 0.146
$\text{CeSi}_{1.9}\text{B}_{0.1}$	<i>I4<sub>1</sub>/amd</i>	$\alpha\text{-ThSi}_2$	4.1878(2)		13.8756(9)	0.055, 0.135
$\text{CeSi}_{1.8}\text{B}_{0.2}$	<i>Imma</i>	$\alpha\text{-GdSi}_2$	4.1879(2)	4.1802(2)	13.8697(6)	0.074, 0.162
$\text{CeSi}_{1.6}\text{B}_{0.4}$	<i>Imma</i>	$\alpha\text{-GdSi}_2$	4.1901(3)	4.1264(3)	13.8798(8)	0.068, 0.159
$\text{CeSi}_{1.5}\text{B}_{0.5}$	<i>P6/mmm</i>	$\text{AlB}_2$	3.9804(1)		4.3040(2)	0.045, 0.144

Small and irregular platelet-shaped single crystals for single-crystal X-ray investigation were selected from the crushed arc-melted sample with the nominal composition  $\text{CeSi}_{1.5}\text{B}_{0.5}$ . Single-crystal XRD data of a representative single-crystalline specimen were collected at room temperature on a Bruker D8 Venture diffractometer with monochromated  $\text{Mo-K}\alpha$  radiation ( $\lambda = 0.71073$  Å). The raw frames data were integrated using the Bruker APEX3 software package. The integrated intensities were corrected for absorption effects using the multiscan method (SADABS) [26]. The symmetry check of the *E* statistics indicated centrosymmetry of the crystal structure and an analysis of high versus lower indices Laue classes was performed. The starting atomic parameters were initially derived via direct methods using the program Sir97 [27] and

subsequently refined with the program SHELXL97 employing the WinGX program package [28, 29] (full-matrix least-squares on  $F^2$ ) allowing anisotropic displacements parameters. The refinement confirmed the  $\text{CeSi}_{1.5}\text{B}_{0.5}$  composition. All relevant details concerning the data collection are listed in Table 2. The program Diamond was used for the drawing of the crystal structure [30].

**Table 2**

Single crystal crystallographic data for  $\text{CeSi}_{1.5}\text{B}_{0.5}$ .

Empirical formula	$\text{CeSi}_{1.5}\text{B}_{0.5}$
Crystal system	Hexagonal
Space group	$P6/mmm$ (No. 191)
Pearson symbol	$hP3$
Lattice parameters	
$a$ , Å	3.9922(2)
$c$ , Å	4.3053(4)
Unit cell volume $V$ , Å <sup>3</sup>	59.424(8)
Calculated density, g cm <sup>-3</sup>	5.292
Absorption coefficient, cm <sup>-1</sup>	19.519
Crystal size, mm <sup>3</sup>	0.12 x 0.09 x 0.02
Radiation and wavelength, Å	Mo $K\alpha$ , 0.71069
Diffractometer	Bruker D8 Venture
Refined parameters, refinement	7, $F^2$
$2\theta_{\text{max}}$ and $(\sin\theta/\lambda)_{\text{max}}$	72.13, 0.828
$h, k, l$	$-6 < h < 6, -6 < k < 6, -7 < l < 7$
Collected reflections	973
Independent reflections	191 ( $R_{\text{int}} = 0.049$ )
Reflections with $I_o > 2\sigma(I_o)$	191 ( $R_{\sigma} = 0.035$ )
Final $R_1$ indices ( $R_1$ all data) <sup>a</sup>	0.019 (0.019)
Weighted $wR_2$ factor ( $wR_2$ all data) <sup>b</sup>	0.041 (0.041)
Goodness-of-fit on $F^2$	1.16
Largest diff. peak and hole / ( $e^{-}/\text{Å}^{-3}$ )	-1.43/1.43

<sup>a</sup> $R_1(F^2) = [(|F_o| - |F_c|)]/|F_o|$ . <sup>b</sup> $wR_2(F^2) = [w(F_o^2 - F_c^2)^2/[w(F_o^2)^2]]^{1/2}$ ;  $[w^{-1} = \sigma^2(F_o)^2 + (0.0104P)^2]$ , where  $P = (F_o^2 + 2F_c^2)/3$ .

### 2.3. Low temperature physical properties

Temperature and field dependent magnetic measurements were performed on a SQUID MPMS, (Quantum Design, San Diego, CA) magnetometer (from 2 K to room temperature) applying static magnetic fields up to 6 T. Four-point electrical resistances as a function of

temperature were measured with the ac option available in a PPMS device (Quantum Design) using current between 1 and 10 mA and frequencies of 19 Hz and 119 Hz.

#### 2.4. Electronic structure calculations

Spin-polarized density functional theory (DFT) calculations were carried out in order to gain insight into the structural and electronic properties of the alloys  $\text{CeSi}_{2-x}\text{B}_x$  ( $x = 0$  and  $0.5$ ). Starting from the experimental lattice parameters and atomic positions published in the literature for  $x = 0$  and our data for  $x = 0.5$ , the crystal structures were optimized. Full occupation of the Si positions was assumed. The full-potential linearized augmented plane wave (FLAPW) approach, as implemented in the *WIEN2K* code [31, 32, 33] was employed. The Perdew, Burke and Ernzerhof (PBE) functional [34] and a plane wave cut-off corresponding to  $R_{MTK_{max}} = 7$  were used. The radial wave functions inside the non-overlapping muffin-tin spheres were expanded up to  $l_{max} = 12$ . The charge density was Fourier expanded up to  $G_{max} = 12 \text{ \AA}^{-1}$ . The muffin-tin radii were set to 1.94, 2.50, and 1.94 a.u. for B, Ce, and Si atoms, respectively. Total energy convergence was achieved with a Brillouin Zone (BZ) integration mesh of 500  $k$ -points, generating 144  $k$ -points in the irreducible part of the BZ. For a better description of the localized  $4f$  states of the rare-earth element Ce, all electronic densities of states (DOS) were computed using the PBE0 hybrid functional [35] and including spin-orbit coupling (SO) [36], with a magnetization confined along the [001] direction. Electronic density of states (DOS) were plotted considering the Fermi level as the energy reference.

When possible, two approaches were used to probe the thermodynamical stability of  $\text{CeSi}_{2-x}\text{B}_x$  ( $x = 0$  and  $0.5$ ) in the three structure types ( $\alpha$ - $\text{GdSi}_2$ ,  $\alpha$ - $\text{ThSi}_2$  and  $\text{AlB}_2$ ): i) The theoretical phonon spectra were calculated using density functional perturbation theory (DFPT) [37] as implemented in the *PHONOPY* package [37], and ii) The PBE+ $U$  [38] energies were used as the fitness function of the evolutionary algorithm *USPEX* [39]. A fixed-composition calculation was applied for the  $\text{CeSi}_2$  and  $\text{CeSi}_{1.5}\text{B}_{0.5}$  phases (12 atoms per unit cell), and up to 1200 and 2000

structural optimizations were performed, respectively. PBE+ $U$  calculations were carried out since they are much faster than PBE0 calculations that could not be envisioned for so many structural optimizations. The first-generation structures were created randomly, and a population of 60 was employed in this work. The best 70% of each generation were used to produce the next generation structures by heredity. Global optimizations were performed for at least 15 generations after the minimum energy was found. In any mode, no initial assumption about the crystal structure of the known phases was implied. All phases were calculated with the same  $U_{\text{eff}}$  value, which allowed for direct comparison of the calculated enthalpies of formation. The final structural parameters reported were obtained from the *FINDSYM* algorithm [40], using a tolerance of 0.10 Å. Thus, periodic DFT calculations were performed on these different structures of these compounds using the *VASP* code [41, 42]. Because of the presence of localized 4*f*-electrons, an additional Hubbard-like term was introduced for Ce. The simplified Dudarev approach [43] was employed with  $U_{\text{eff}} = U - J = 5$  eV for the Ce 4*f* atomic orbitals. The exchange-correlation interaction was described within the generalised gradient approximation in the parametrisation of the PBE functional [35]. Projector augmented wave potentials were used for all atoms [44] and calculations were performed with a cut-off energy of 400 eV. The electronic wave functions were sampled on dense densities in the irreducible BZ using the Monkhorst–Pack method [45]. Structure relaxations including cell parameters and atomic positions were carried out without any symmetry constraints.

### 3. Results and discussion

#### 3.1. Structural characterization

The X-ray powder patterns of the boron-containing alloys  $\text{CeSi}_{2-x}\text{B}_x$  ( $x = 0, 0.1, 0.2, 0.4,$  and  $0.5$ ) were indexed on the basis of tetragonal, orthorhombic and hexagonal symmetry of the  $\alpha$ - $\text{ThSi}_2$ ,  $\alpha$ - $\text{GdSi}_2$  and  $\text{AlB}_2$  type structures, respectively. Partial substitution of Si by B changes the initial structure. In order to check the homogeneity of the sample, Rietveld profile refinements of

the X-ray powder patterns were performed using the program *WinCSD* [25]. The PXRD patterns collected of  $\text{CeSi}_2$  and  $\text{CeSi}_{1.9}\text{B}_{0.1}$  indicated homogeneous phases of  $\alpha\text{-ThSi}_2$ -type structure. For the  $\text{CeSi}_{1.8}\text{B}_{0.2}$  and  $\text{CeSi}_{1.6}\text{B}_{0.4}$  compositions, the  $\alpha\text{-GdSi}_2$ -type structure was found, whereas for  $\text{CeSi}_{1.5}\text{B}_{0.5}$ , the  $\text{AlB}_2$ -type structure was observed. The stoichiometric compositions of the binary and Ce/Si ratio for ternary compounds were confirmed by EDX analysis. Crystallographic data for the  $\text{CeSi}_{2-x}\text{B}_x$  ( $x = 0, 0.1, 0.2, 0.4, \text{ and } 0.5$ ) are given in [Table 1](#). [Fig. 1](#) illustrates the final Rietveld refinement obtained between the calculated and observed patterns of the sample  $\text{CeSi}_{1.5}\text{B}_{0.5}$  which crystallizes in the  $\text{AlB}_2$ -type of structure. Small traces of  $\text{CeB}_4$  [46] were detected in the alloy  $\text{CeSi}_{1.5}\text{B}_{0.5}$  by means of EDX and PXRD analysis.

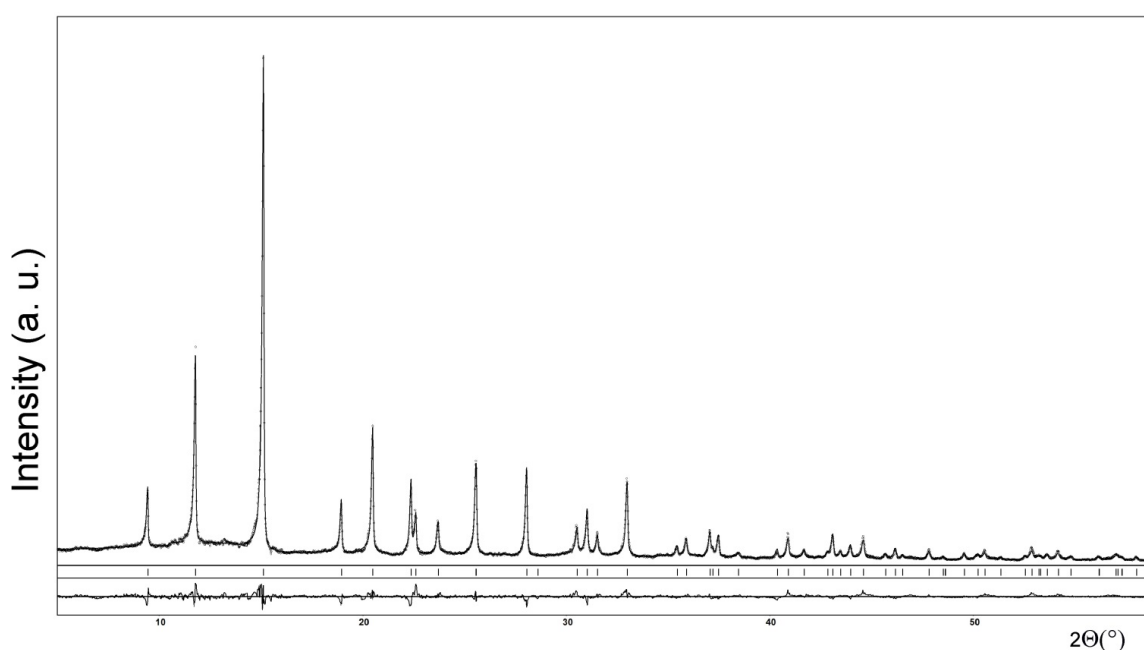


**Fig. 1.** Comparison of observed and calculated X-ray powder profiles for  $\text{CeSi}_{1.5}\text{B}_{0.5}$  ( $\text{AlB}_2$  type structure).

A high-quality single crystal could be obtained via mechanical fragmentation of the sample with nominal composition  $\text{CeSi}_{1.5}\text{B}_{0.5}$ . Details of the single crystal X-ray analysis and crystal data are compiled in [Table 2](#). The atomic coordinates and the thermal displacement factors are listed in [Table 3](#).

**Table 3**

Atomic coordinates and displacement parameters<sup>a</sup> (in  $\text{\AA}^2$ ) for  $\text{CeSi}_{1.5}\text{B}_{0.5}$ .

Atom	Site	SOF	$x/a$	$y/b$	$z/c$	$U_{eq}/U_{iso}$	$U_{11}=U_{22}$	$U_{33}$	$U_{12}$
Ce	1( <i>a</i> )	1.00	0	0	0	0.0075(2)	0.00741(14)	0.00787(16)	0.00370(7)
Si	2( <i>d</i> )	0.75(2)	2/3	1/3	1/2	0.0168(6)	0.0196(8)	0.0112(8)	0.0098(4)
B	2( <i>d</i> )	0.25(2)	2/3	1/3	1/2	0.0168(6)	0.0196(8)	0.0112(8)	0.0098(4)

$${}^a U_{23} = U_{13} = 0.$$

An attempt to refine the structure with complete occupation of both positions (cerium and silicon) led to  $R_{1(iso)} = 0.025$  in the isotropic and  $R_{1(aniso)} = 0.023$  for the anisotropic approximation of atomic displacement. Despite quite acceptable values of the residual factors, our results indicate large values of the anisotropic displacement parameters for  $U_{11}$  for Si atoms. A refinement of the site occupancy for the silicon position ( $SOF(Si)$ ) and subsequent refinement of the atomic displacement parameters led to slightly smaller residual values ( $R_{1(iso)} = 0.022$  and  $R_{1(aniso)} = 0.019$ ) and an occupation factor  $SOF(Si) = 0.843(1)$ , but with a more reasonable ratio of  $U_{eq}(Ce)/U_{eq}(Si)$ . Taking this into account, the presence of boron leads to a mixed Si/B occupied position 2*d* with a Si/B ratio of 75(2)/25(2). Consequently, the refined composition of the investigated phase indicates the formula  $CeSi_{1.5}B_{0.5}$ . The corresponding Ce/Si ratio of the latter of 40/60 matches with the nominal composition ratio found by EDX analysis which is 39.1/60.9.

The lattice parameter  $a = 3.9922(2)$  Å reflects the nearest Ce–Ce distances (see Fig. 2). Ce–Si/B distances are found to be 3.154(1) Å. With the covalent radii of silicon (1.17 Å) and boron (0.85 Å) [47], the interatomic distances for Si/B–Si/B (2.3049(1) Å) measured within the hexagon clearly indicates the presence of boron in the structure.

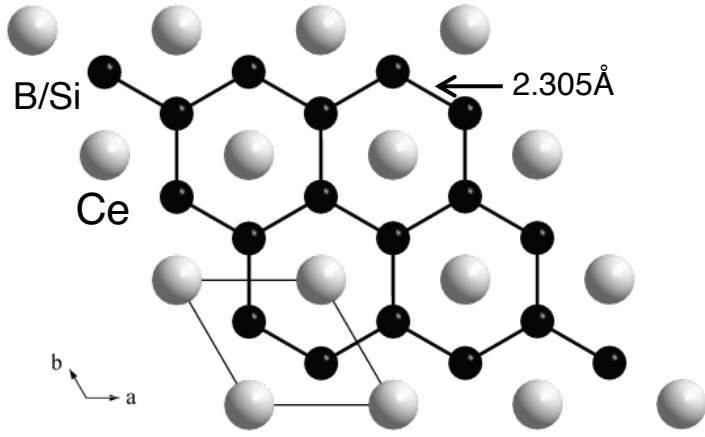


**Fig. 2.** Crystal structure of  $\text{CeSi}_{1.5}\text{B}_{0.5}$  ( $\text{AlB}_2$ -type). Large grey and small black balls are Ce and B/Si atoms, respectively.

### 3.2. Magnetic and electrical properties

The molar magnetic susceptibilities measured in an external magnetic field of 100 Oe exhibit a hysteresis between the field cooled (fc) and the zero-field cooled (zfc) susceptibility for samples with a B content  $x > 0.5$ , typically below  $\sim 15$  K, indicating correlated magnetic behavior. For the sample  $\text{CeSi}_{1.8}\text{B}_{0.2}$  (Fig. 3 (c)), the fc susceptibility exhibits the characteristics of a ferromagnet with a Curie temperature of  $\sim 14$  K. The phases with  $x = 0$  and  $x = 0.1$  (Fig. 3 (a) and (b)) do not show indication of long-range order at low temperatures. Their inverse susceptibilities at high temperatures ( $T > 200$  K) follow Curie-Weiss laws given by

$$C = \frac{N_A \mu_0 \mu_B^2 \mu_{\text{eff}}^2}{3k_B(T - \Theta_{\text{CW}})} + \chi_0 \quad \text{eq. (1)}$$

where  $N_A$  is the Avogadro constant,  $\mu_B$  the Bohr magneton,  $k_B$  the Boltzmann constant,  $\mu_{\text{eff}}$  the effective magnetic moment and  $\Theta_{\text{CW}}$  the Curie-Weiss temperature, the latter two quantities being fit parameters.

For the temperature independent susceptibility,  $\chi_0$ , we used the diamagnetic increments of  $\text{Ce}^{3+}$  and  $\text{Si}^{4+}$  listed by Bain and Berry [48]. The Curie-Weiss temperatures (see Table 4) are of the order of  $\sim -100$  K. At low temperatures, the inverse susceptibilities gradually bend in and vanish towards lowest temperatures. This temperature dependence is typical for crystal field

splitting effects which in the case of  $\text{Ce}^{3+}$  split the  ${}^2F_{5/2}$  Russel-Saunders ground state of the  $4f^1$  electronic configuration into three Kramers doublets. By further substituting boron and entering the  $\alpha\text{-GdSi}_2$  structure-type, the inverse susceptibilities become less curved (Fig. 3 (c), (d)), indicating a reduction of the crystal electric field splitting, possibly also due to a random variation of the Si/B environment to the Ce atoms. The fits of a Curie-Weiss law to the inverse susceptibilities resulted in effective magnetic moments of  $\sim 2.7 - \sim 2.9 \mu_{\text{B}}$  (see Table 4), somewhat higher than expected for  $\text{Ce}^{3+}$  with electronic configuration  $4f^1$  ( $2.54 \mu_{\text{B}}$ ) [49].

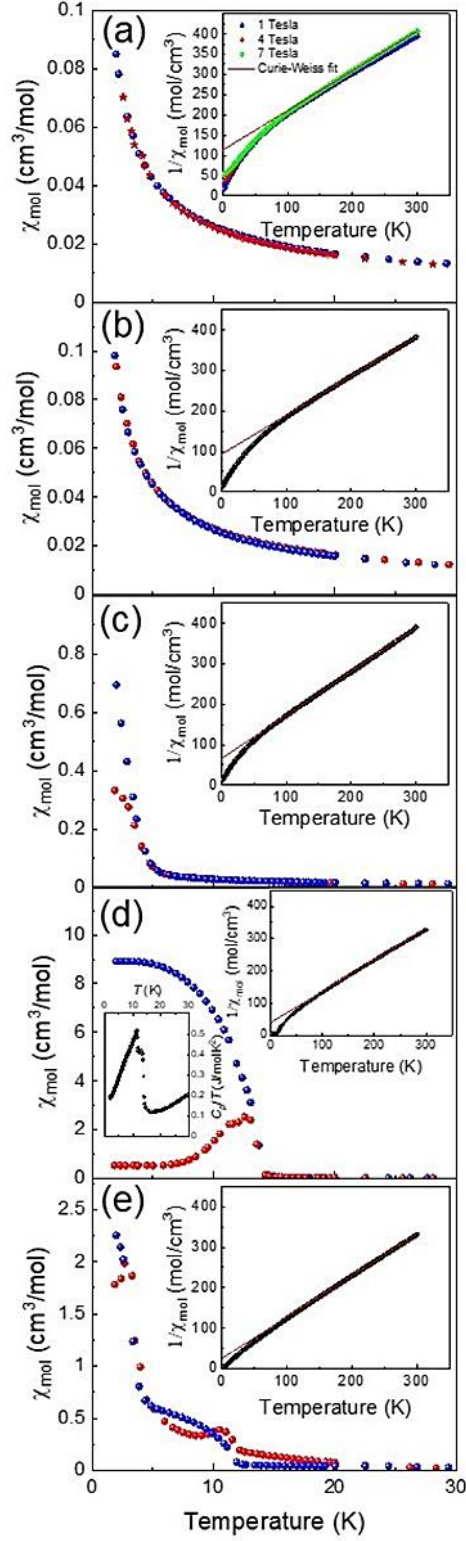


**Fig. 3.** Molar magnetic susceptibilities for the samples  $\text{CeSi}_{2-x}\text{B}_x$  ( $x = 0, 0.1, 0.2, 0.4, 0.5$ ) (from top to bottom). The main frames display the zero-field cooled (zfc, red dots) and the field-cooled susceptibilities (fc, blue dots) collected in an external magnetic field of 100 Oe. The insets show the inverse susceptibilities taken in an external field of 10 kOe (for (b), (c), (d), and (e)). The solid red lines are fits to a Curie-Weiss law with parameters compiled in Table 4. For (a) the susceptibilities reveal a slight magnetic field dependence, possibly due to minute traces of a ferromagnetic impurity. The Curie-Weiss fit was performed using the data collected at 7 T. The left inset in (c) displays the low-temperature specific heat capacity of  $\text{CeSi}_{1.6}\text{B}_{0.4}$ .

**Table 4.** Effective magnetic moments,  $\mu_{\text{eff}}$ , Curie-Weiss temperatures,  $\Theta_{\text{CW}}$ , and magnetic entropies (see text) of the phases  $\text{CeSi}_{2-x}\text{B}_x$  obtained from fits to the high-temperature ( $T \geq 200$  K) magnetic susceptibilities according to eq. (1) and the integration of  $C_{\text{mag}}(T)/T$ . The temperature independent diamagnetic susceptibility contribution,  $\chi_0$ , in eq. (1) arising from the electrons in the closed shells was calculated from Pascal’s increments and fixed to  $-22 \times 10^{-6}$   $\text{cm}^3/\text{mol}$  [48].

Fig. 3	phase	$\mu_{\text{eff}}(\mu_{\text{B}})$	$\Theta_{\text{CW}}$ (K)	$S_{\text{mag}}/R \ln 2$ (%)
(a)	$\text{CeSi}_2$	2.87	-117	-
(b)	$\text{CeSi}_{1.9}\text{B}_{0.1}$	2.88	-96	-
(c)	$\text{CeSi}_{1.8}\text{B}_{0.2}$	2.74	-62	47
(d)	$\text{CeSi}_{1.6}\text{B}_{0.4}$	2.89	-42	80
(e)	$\text{CeSi}_{1.5}\text{B}_{0.5}$	2.81	-25	80

The low-field susceptibilities of the phases with  $x > 0.2$  (Fig. 3(c) – (e)) exhibit anomalies associated to cooperative magnetic behavior at low temperatures. Especially well developed is the anomaly for the phase  $\text{CeSi}_{1.6}\text{B}_{0.4}$  (see the low-temperature specific heat displayed in the left inset in Fig. 3d). It exhibits a slight splitting, also visible in the field-cooled magnetic susceptibility, which may be ascribed to a random environment of the magnetic entities. The specific heat of the  $\text{AlB}_2$  phase  $\text{CeSi}_{1.5}\text{B}_{0.5}$  (not shown) shows a rounded peak centred at 2.6 K, coinciding well with the low temperature peaks in the magnetic susceptibilities. Integrating the magnetic contributions to the heat capacities  $C_{\text{mag}}(T)/T$  of the phases  $\text{CeSi}_{1.6}\text{B}_{0.4}$  and  $\text{CeSi}_{1.5}\text{B}_{0.5}$  obtained after a subtraction of an appropriate lattice contribution to the heat capacity, results in a magnetic entropy contained in the anomaly of  $\sim 80$  % of  $R \ln 2$ , with  $R$  being the molar gas constant (see Table 4). This result implies ordering of a Kramers doublet ground state resulting from the crystal electric field splitting of the 6-fold degenerate  ${}^2F_{5/2}$  Russel-Saunders multiplet expected for the  $4f^1$  electronic configuration [50, 51]. For the phase  $\text{CeSi}_{1.8}\text{B}_{0.2}$ ,  $C_p/T$  (not shown) increases towards lowest temperatures indicating that magnetic correlation energies are well

below  $\sim 2$  K and the magnetic entropy amounts to only 47 % of the entropy  $R \ln 2$  expected for a Kramers doublet.

Measurements of the electrical resistance indicate metallic conductivity for all phases with typical resistivities of the order of  $100 \mu\Omega\text{cm}$ , except for the phase  $\text{CeSi}_{1.6}\text{B}_{0.4}$  for which the resistivity was found to be an order of magnitude larger (Fig. 4). The temperature dependences of the resistivities, especially of the phases with  $x \geq 0.2$  exhibit anomalies at low temperatures which we ascribe to magnetic scattering of the electrons with the Ce magnetic moments. For the phase  $\text{CeSi}_{1.6}\text{B}_{0.4}$ , the resistivity shows a sharp spike with maximum at 14 K, coinciding well with the magnetic ordering anomalies found in the magnetic susceptibility measurements. The resistivities of the phases with  $x < 0.2$  after an almost flat plateau above  $\sim 200$  K decrease continuously. The resistivity of  $\text{CeSi}_2$  exhibits a step-like feature at about 260 K, the origin of which is unclear at present.

Summarizing the electrical and magnetic properties, the phases  $\text{CeSi}_{2-x}\text{B}_x$  ( $x = 0, 0.1, 0.2, 0.4, 0.5$ ) are metallic and phases with B substitution  $x \geq 0.2$  exhibit magnetic correlated behavior, typically below  $\sim 15$  K. The magnetic contributions to the specific heat indicate Kramers doublets as the crystal field ground states. Indications of magnetic order above  $\sim 1.9$  K are not observed for the phases with  $x < 0.2$ . Here, the magnetic susceptibilities show a temperature dependence characteristic of a crystal electric field split multiplet of three Kramers doublets. The high temperature susceptibilities of all phases indicate the Ce cations to be in an oxidation state +3 with the effective magnetic moments slightly higher than expected value of  $2.54 \mu_B$ .

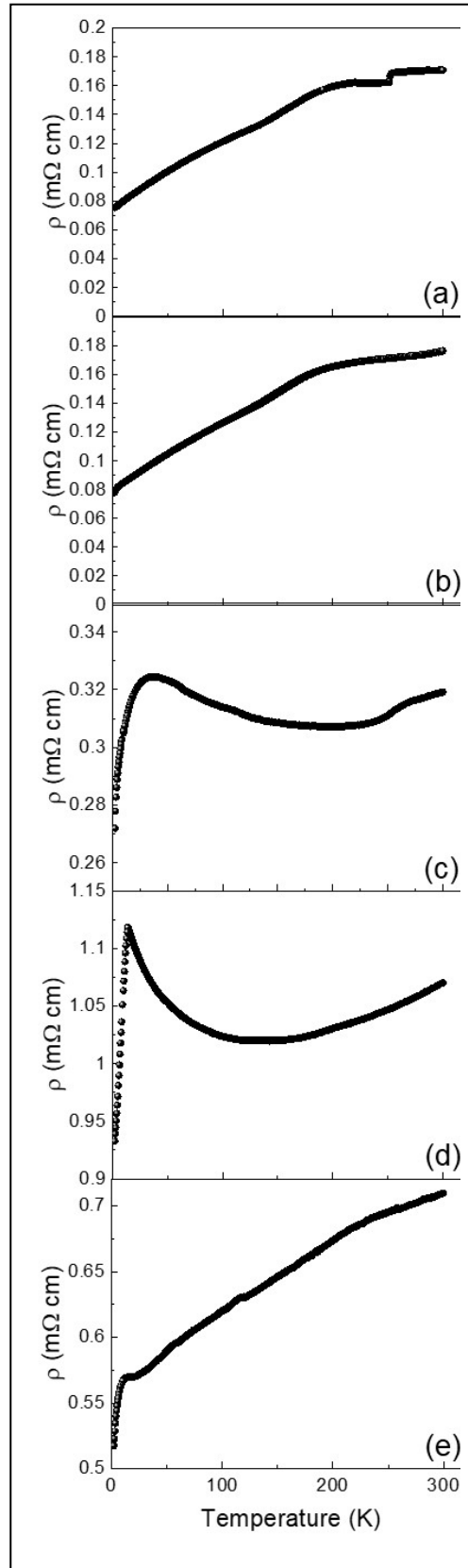


**Fig. 4** Electrical resistivities ( $\rho$ ) of the phases  $\text{CeSi}_{2-x}\text{B}_x$  ( $x = 0, 0.1, 0.2, 0.4, 0.5$ ) (from top to bottom).

### 3.3. Electronic structure properties

DFT calculations were initially carried out on stoichiometric  $\text{CeSi}_2$  in the three type structures (orthorhombic  $\alpha\text{-GdSi}_2$  ( $Imma$ ), tetragonal  $\alpha\text{-ThSi}_2$  ( $I4_1/amd$ ), and hexagonal  $\text{AlB}_2$  (SG  $P6/mmm$ )) in order to gain some insight on its structural and electronic properties. The structural arrangements were optimized (see [Table S1](#) for the pertinent structural optimized parameters) and their relative energies compared. Interestingly, the three arrangements are almost isoenergetic. Indeed, both  $\alpha\text{-GdSi}_2$  (SG  $Imma$ ) and  $\alpha\text{-ThSi}_2$  (SG  $I4_1/amd$ ) arrangements are strictly isoenergetic whereas the  $\text{AlB}_2$  (SG  $P6/mmm$ ) is hardly less stable by less than 5 kJ/mol per  $\text{CeSi}_2$  motif. Given the  $\text{CeSi}_2$  structural motif, to find equal for the  $\alpha\text{-GdSi}_2$  (SG  $Imma$ ) and  $\alpha\text{-ThSi}_2$  (SG  $I4_1/amd$ ) arrangements energies is not too surprising, since they exhibit an alike local atomic environment. Finding similar energies for the  $\text{AlB}_2$ -type (SG  $P6/mmm$ ) is more unexpected (see [Fig. 5](#)).

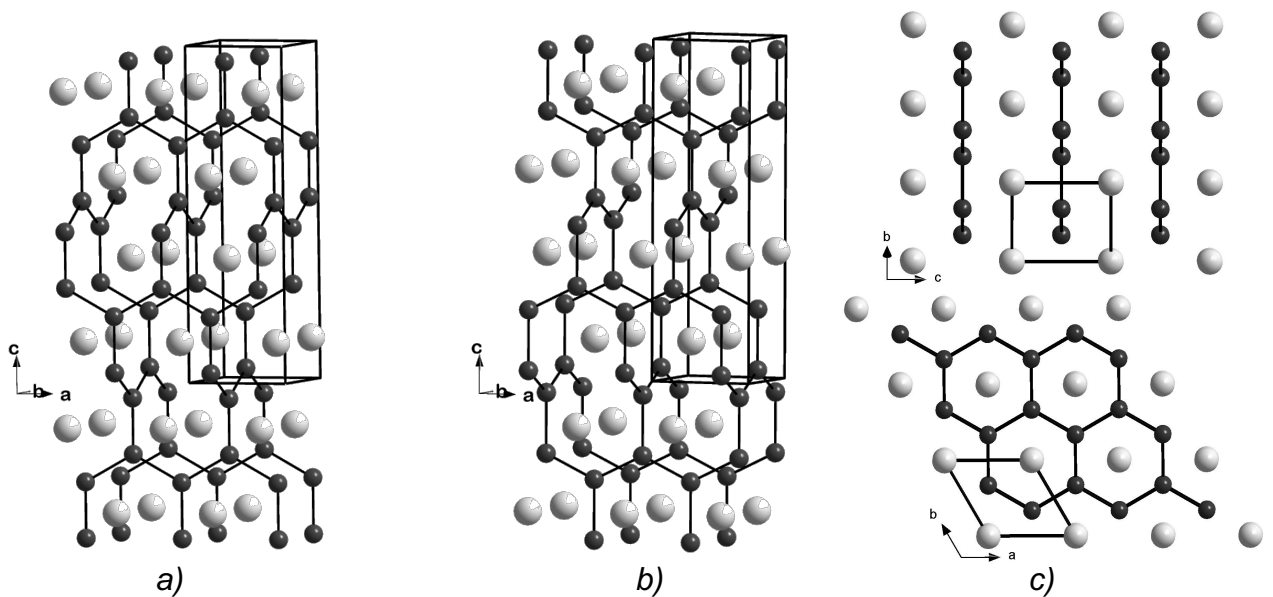


**Fig. 5.** DFT-optimized structural arrangements of  $\text{CeSi}_2$  with (a) the  $\alpha\text{-GdSi}_2$  ( $Imma$ ), (b)  $\alpha\text{-ThSi}_2$  ( $I4_1/amd$ ), and (c)  $\text{AlB}_2$  ( $P6/mmm$ ) structure-types. Large grey and small black balls are Ce and Si atoms, respectively.

To investigate the thermodynamical stability of  $\text{CeSi}_2$  within the set of the three structural arrangements further, the phonon density of states (DOS) and phonon dispersion relations along some high-symmetry lines in the first BZ (see the right hand-side of [Fig. 6](#) for the corresponding BZ) were calculated. They are shown in [Fig. 6](#). As expected, acoustic low frequency modes

mostly involve cerium vibrations. They are comparable in the three arrangements (slightly more energy broadening is observed for the  $\alpha$ -ThSi<sub>2</sub> ( $I4_1/amd$ ) arrangement). Hardly any imaginary phonon frequencies are observed, indicating that the three arrangements are thermodynamically stable at 0 K. This finding suggests that slight off-stoichiometry is the reason why experimentally, Bulanova *et al.* found the cerium disilicide CeSi<sub>2-x</sub> with either  $\alpha$ -GdSi<sub>2</sub> structure type ( $Imma$ ) or the  $\alpha$ -ThSi<sub>2</sub> structure type (SG  $I4_1/amd$ ), depending upon the  $x$  value [16].

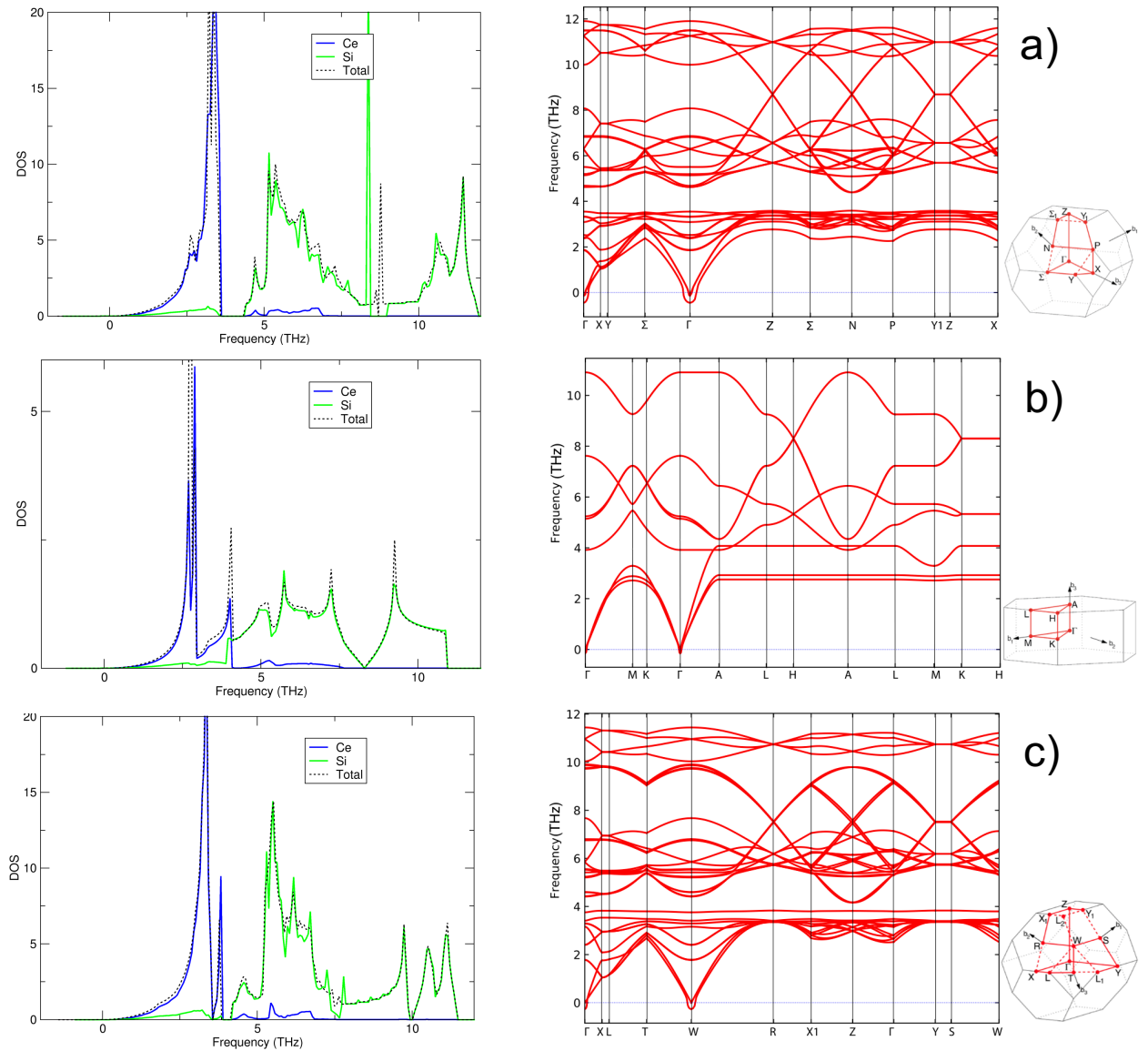
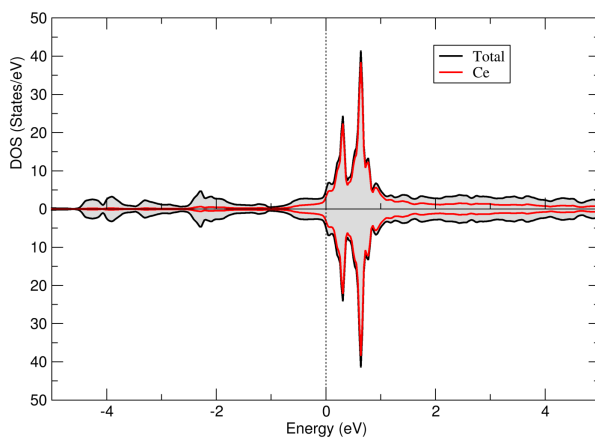
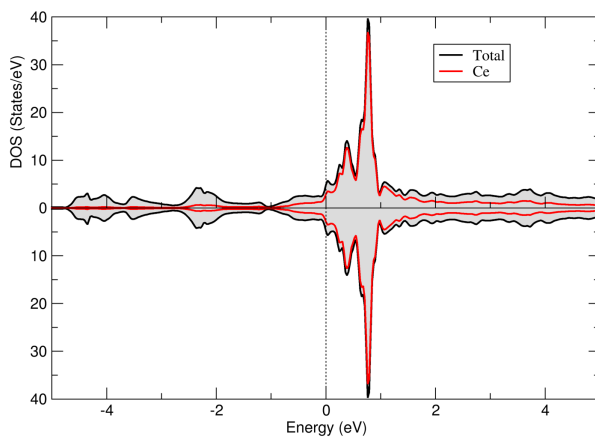


**Fig. 6.** Total and atom-projected phonon density of states (DOS in states/THz/cell) (left) and phonon band dispersion (right) for CeSi<sub>2</sub> with (a) the  $\alpha$ -GdSi<sub>2</sub> ( $Imma$ ), (b)  $\alpha$ -ThSi<sub>2</sub> ( $I4_1/amd$ ), and (c) AlB<sub>2</sub> ( $P6/mmm$ ) structural arrangements.

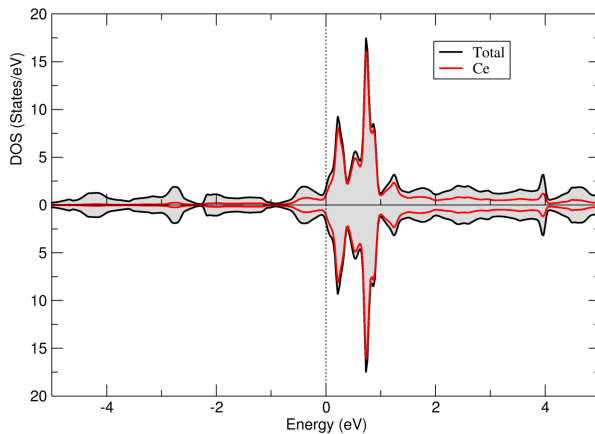
The computed total and atom-projected spin-polarized electronic DOS are sketched in Fig. 7. They are rather dispersed between from  $-5$  to  $5$  eV, except the Ce  $4f$ -band localized above the Fermi level ( $\varepsilon_F$ ), hardly spin-polarized, with  $\varepsilon_F$  lying in a low peak of DOS made of mostly Ce ( $4d$ ) contribution with a little admixture of Si. The spin-up and spin-down  $f$ -orbital projected DOS seem to be both empty overall, indicating rather a formal  $4f^0$  electronic configuration.



a)



b)



c)

**Fig. 7.** Total and atom-projected spin-polarized PBE0+SO electronic DOS of  $\text{CeSi}_2$  with (a) the  $\alpha\text{-GdSi}_2$  ( $Imma$ ), (b)  $\alpha\text{-ThSi}_2$  ( $I4_1/amd$ ), and (c)  $\text{AlB}_2$  ( $P6/mmm$ ) structural arrangements. Fermi level ( $\epsilon_F$ ) set at 0 eV.

DFT calculations were then carried out on the ternary  $\text{CeSi}_{1.5}\text{B}_{0.5}$  compound where part of Si atoms was substituted by some boron atoms, hoping to get information allowing to analyze the differences and similarities with the binary  $\text{CeSi}_2$  compound. Three arrangements were considered which were derived from the  $\alpha\text{-GdSi}_2$  (SG  $Imma$ ),  $\alpha\text{-ThSi}_2$  (SG  $I4_1/amd$ ), and  $\text{AlB}_2$  (SG  $P6/mmm$ ) structural arrangements – a specific ‘coloring’ was chosen for each of them (see Fig. 8) with SG  $Imm2$ ,  $Imm2$ , and  $P6/mmm$  ‘true’ symmetry, respectively ( $Z = 4$  for all of them).

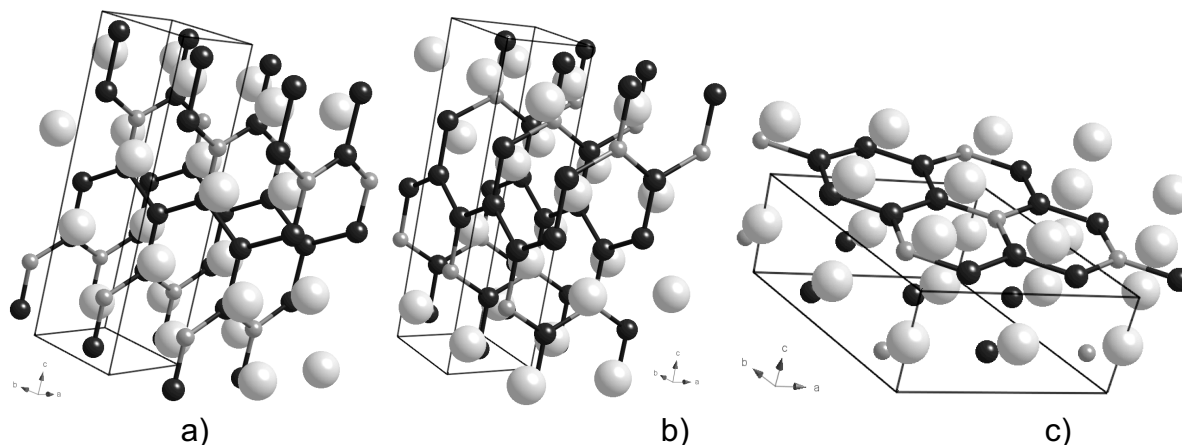
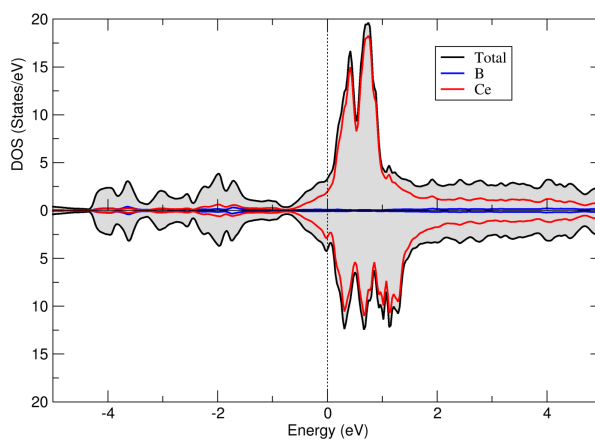


**Fig. 8.** DFT-optimized structural arrangements of  $\text{CeSi}_{1.5}\text{B}_{0.5}$  with (a) the  $\alpha\text{-GdSi}_2$ -derived ( $Imm2$ ), (b)  $\alpha\text{-ThSi}_2$ -derived ( $Imm2$ ), and (c)  $\text{AlB}_2$ -derived ( $P6/mmm$ ) structure-types. Large grey, black, and small grey balls are Ce, Si, and B atoms, respectively.

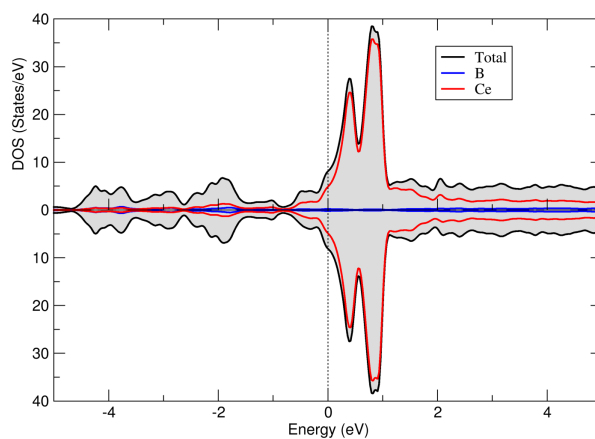
A comparison of the relative energies of these three optimized arrangements (see Table S1 for the pertinent structural optimized parameters) indicates, as for the binary  $\text{CeSi}_2$ , that they are rather close in energy, but this time in favor of the  $\text{AlB}_2$ -derived arrangement (SG  $P6/mmm$ ) in agreement with experiments (relative energies (kJ/mol) per  $\text{CeSi}_{1.5}\text{B}_{0.5}$  motif: 4.6, 4.0, and 0 for SG  $Imm2$ ,  $Imm2$ , and  $P6/mmm$  arrangements). Additionally, a structure search for  $\text{CeSi}_{1.5}\text{B}_{0.5}$ , combining DFT computations and the evolutionary algorithm USPEX (see above for the computational details), produced also the  $\text{AlB}_2$ -derived arrangement (SG  $P6/mmm$ ) as the most

probable at ambient pressure (see Fig. S1). These results support the experiments showing that incorporation of boron induces a phase transformation of the cerium disilicides.

The computed total and atom-projected spin-polarized electronic DOS of the arrangements are sketched and compared in Fig. 9. Those for the  $\alpha$ -ThSi<sub>2</sub>-derived (SG *Imm2*), and the most stable AlB<sub>2</sub>-derived (SG *P6/mmm*) structure types are hardly polarized and resemble those of the corresponding binaries. On the other hand, the DOS of the  $\alpha$ -GdSi<sub>2</sub>-derived (SG *Imm2*) structure-type is somewhat spin-polarized, pointing to some exchange interaction and magnetic correlations.



a)



b)

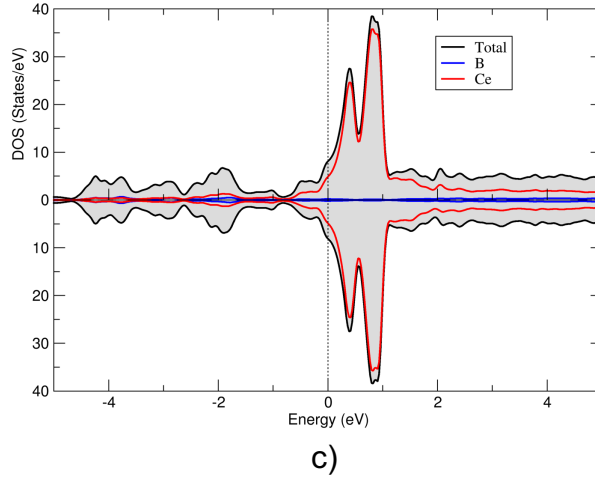


**Fig. 9.** Total and atom-projected spin-polarized PBE0+SO electronic DOS of  $\text{CeSi}_{1.5}\text{B}_{0.5}$  with (a) the  $\alpha\text{-GdSi}_2$ -derived ( $Imm2$ ), (b) the  $\alpha\text{-ThSi}_2$ -derived ( $Imm2$ ), and (c) the  $\text{AlB}_2$ -derived ( $P6/mmm$ ) structure-types. Fermi level ( $\epsilon_F$ ) set at 0 eV.

#### 4. Conclusion

In this work, the effect of boron insertion in the structural and the physical properties of cerium disilicides was investigated. Samples of the alloys  $\text{CeSi}_{2-x}\text{B}_x$  with different contents of boron ( $x = 0, 0.1, 0.2, 0.4, \text{ and } 0.5$ ) were prepared and their crystal structures, electrical and magnetic properties were determined. The analysis of the data which could be collected, indicated that, depending on the amount of boron the phases  $\text{CeSi}_{2-x}\text{B}_x$  crystallize either in the  $\alpha\text{-ThSi}_2$  structure type ( $x = 0, 0.1$ ) or in the closely related  $\alpha\text{-GdSi}_2$  structure type ( $x = 0.2, 0.4$ ). Interestingly, for  $x = 0.5$ , the crystal structure of  $\text{CeSi}_{1.5}\text{B}_{0.5}$  solved by means of X-ray single crystal diffraction crystallizes in the  $\text{AlB}_2$  structure type. Measurements of the electrical and magnetic properties indicated that phases  $\text{CeSi}_{2-x}\text{B}_x$  ( $x = 0, 0.1, 0.2, 0.4, 0.5$ ) are metallic and that phases with B substitution  $x \geq 0.2$  exhibit magnetic correlated magnetic behavior, typically below  $\sim 15$  K. DFT calculations were performed to elucidate the change of electronic and physical properties upon boron substitution.

#### Declaration of competing interest

The authors declare that they have no known competing financial interests or personal relationships that could have appeared to influence the work reported in this paper.

## Acknowledgments

The authors gratefully thank Dr. V. Smetana (Stockholm University, Sweden) for X-ray intensity data collection and E. Brücher (Max-Planck-Institut für Festkörperforschung) for the magnetization and resistance measurements.

## Appendix A. Supplementary data

Supplementary data to this article can be found online at <https://doi.org/10.1016/j.solidstatesciences...>

## References

- [1] Yu. Kuz'ma, N. F. Chaban *Binary and Ternary Systems Containing Boron*; Metallurgiya, Moscow, 1990 (in Russian).
- [2] N. F. Chaban, Yu. B. Kuz'ma, Phase equilibria in the Er-Si-B system, *Inorg. Mater.* 2000, 36, 1057–1058, <https://doi.org/10.1007/BF02758697>
- [3] N. F. Chaban, Yu. B. Kuz'ma, X-ray Diffraction Study of the RMB (R= Y, La, Ce; M= Al, Si) Systems, *Dopov. AN. URSR*, 11 (1971) 1048–1050 (in Ukrainian).
- [4] R. Jardin, V. Babizhetskyy, R. Guérin, J. Bauer, Crystal structure of the rare earth borosilicide  $\text{Er}_8\text{Si}_{17}\text{B}_3$ , *J. Alloys Compd.* 353 (2003) 233–239, [https://doi.org/10.1016/S0925-8388\(02\)01318-X](https://doi.org/10.1016/S0925-8388(02)01318-X)
- [5] V. Babizhetskyy, V. Levytskyi, R. Jardin, J. Bauer, R. Guérin, R. Gautier, B. Fontaine, J.-F. Halet, Rare-earth metal borosilicides  $R_9\text{Si}_{15-x}\text{B}_3$  ( $R = \text{Tb, Yb}$ ): new ordered structures derived from the  $\text{AlB}_2$  structure type, *Z. Anorg. Allg. Chem.* 646 (2020) 1168–1175, <https://doi.org/10.1002/zaac.202000046>
- [6] V. Babizhetskyy, R. Jardin, R. Gautier, B. Fontaine, J.-F. Halet, Flux synthesis, crystal structure and electronic properties of the layered rare earth metal boride silicide  $\text{Er}_3\text{Si}_{5-x}\text{B}$ . An example of a boron/silicon-ordered structure derived from the  $\text{AlB}_2$  structure type, *Z. Naturforsch.* 76b (10-12) (2021) 869–879, <https://doi.org/10.1515/znb-2021-0143>
- [7] J. Roger, V. Babizhetskyy, T. Guizouarn, K. Hiebl, J.-F. Halet, R. Guérin, The ternary RE–Si–B systems (RE = Dy, Ho, Er and Y) at 1270 K: Solid state phase equilibria and magnetic properties of the solid solution  $\text{REB}_{2-x}\text{Si}_x$  (RE = Dy and Ho), *J. Alloys Compd.* 417 (2006) 72–84, <https://doi.org/10.1016/j.jallcom.2005.09.012>
- [8] J. Roger, V. Babizhetskyy, K. Hiebl, J.-F. Halet, R. Guérin, Solid state phase equilibria in the ternary Nd–Si–B system at 1270 K, *J. Alloys Compd.* 415 (2006) 73–84, <https://doi.org/10.1016/j.jallcom.2005.07.045>

- [9] V. Babizhetskyy, J. Roger, J. Bauer, S. Députier, R. Jardin, R. Guérin, Solid state phase equilibria in the Gd–Si–B system at 1270 K, *J. Solid State Chem.* 177 (2004) 415–424, <https://doi.org/10.1016/j.jssc.2003.02.011>
- [10] V. Babizhetskyy, J. Roger, S. Deputier, R. Guérin, R. Jardin, J. Bauer, K. Hiebl, C. Jardin, J.-Y. Saillard, J.-F. Halet, Gd<sub>5</sub>Si<sub>2</sub>B<sub>8</sub>: A Ternary Rare-Earth-Metal Silicide Boride Compound, *Angew. Chem. Int. Ed.* 43 (2004) 1979–1983, <https://doi.org/10.1002/ange.200352468>
- [11] J. Roger, V. Babizhetskyy, S. Cordier, J. Bauer, K. Hiebl, L. Le Pollès, E. S. Ashbrook, J.-F. Halet, R. Guérin, Crystal structures, physical properties and NMR experiments on the ternary rare-earth metal silicide boride compounds RE<sub>5</sub>Si<sub>2</sub>B<sub>8</sub> (RE=Y, Sm, Gd, Tb, Dy, Ho), *J. Solid State Chem.* 178 (2005) 1851–1863, <https://doi.org/10.1016/j.jssc.2005.02.023>
- [12] J. Roger, M. Ben Yahia, V. Babizhetskyy, J. Bauer, S. Cordier, R. Guérin, K. Hiebl, X. Rocquefelte, J.-Y. Saillard, J.-F. Halet, Mn<sub>5</sub>Si<sub>3</sub>-type host-interstitial boron rare-earth metal silicide compounds RE<sub>5</sub>Si<sub>3</sub>: Crystal structures, physical properties and theoretical considerations, *J. Solid State Chem.* 179 (2006) 2310–2328, <https://doi.org/10.1016/j.jssc.2006.04.023>
- [13] M. G. Kanatzidis, R. Pöttgen, W. Jeitschko, The metal flux: a preparative tool for the exploration of intermetallic compounds, *Angew. Chem., Int. Ed.* 44 (2005) 6996–7023, <https://doi.org/10.1002/anie.200462170>
- [14] J. Roger, V. Babizhetskyy, R. Jardin, R. Guérin, C. Moinet, U. Burkhardt, J.-F. Halet, Tin flux synthesis of rare-earth metal silicide compounds RESi<sub>1.7</sub> (RE = Dy, Ho): a novel ordered structure derived from the AlB<sub>2</sub> type, *Z. Kristallogr.* 221 (2006) 502–510, <https://doi.org/10.1524/zkri.2006.221.5-7.502>
- [15] W. Hofmann, Jäniche W. Der Strukturtyp von Aluminiumborid (AlB<sub>2</sub>), *Naturwissenschaften*, 23 (1935) 851, <https://doi.org/10.1007/BF01491990>
- [16] M. V. Bulanova, P. N. Zheltov, K. A. Meleshevich, P.A. Saltykov, Cerium–silicon system, *J. Alloys Compd.* 345 (2002) 110–115, [https://doi.org/10.1016/S0925-8388\(02\)00409-7](https://doi.org/10.1016/S0925-8388(02)00409-7)
- [17] M. V. Bulanova, Yu. I. Buyanov, T. Ya. Velikanova, N. P. Horbachuk, V. R. Sidorko. Phase diagram and the phases thermodynamics in binary systems of rare earths and silicon. Kyiv. Naukova Dumka. (in Russian), 2013.
- [18] T. Leisegang, D. C. Meyer, T. Doert, G. Zahn, T. Weißbach, D. Souptel, G. Behr, P. Paufler, *Z. Kristallogr.* 220 (2005) 128–134, <https://doi.org/10.1524/zkri.220.2.128.59116>
- [19] S. A. Shaheen, J. S. Schilling, Ferromagnetism of CeSi<sub>x</sub> at ambient and high pressure, *Phys. Rev. B.* 35 (1987) 6880–6887, <https://doi.org/10.1103/PhysRevB.35.6880>
- [20] W. H. Lee, R. N. Shelton, S. K. Dhar, K. A. Jr. Gschneidner, Competition between the Kondo effect and exchange interactions in the system CeSi<sub>x</sub>, *Phys. Rev. B.* 35 (1987) 8523–8527, <https://doi.org/10.1103/PhysRevB.35.8523>
- [21] J. Pierre, O. Laborde, E. Houssay, A. Rouault, J. P. Senateur, R. Madar, Anisotropy of the magnetic and electrical properties of CeSi<sub>x</sub>, *J. Phys. Cond. Mat.* 2 (1990) 431–441, DOI 10.1088/0953-8984/2/2/018
- [22] H. Yashima, T. Satoh, Nonmagnetic-magnetic transition in Ce-Si system, *Solid Stat. Comm.* 41 (1982) 723–727, [https://doi.org/10.1016/0038-1098\(82\)91125-5](https://doi.org/10.1016/0038-1098(82)91125-5)
- [23] H. Yashima, H. Mori, T. Satoh, K. Kohn, Ferromagnetic dense Kondo behaviour of Ce-Si system, *Solid State Comm.* 43 (1982) 193–197, [https://doi.org/10.1016/0038-1098\(82\)90109-0](https://doi.org/10.1016/0038-1098(82)90109-0)
- [24] U. Burkhardt, V. Gurin, F. Haarmann, H. Borrmann, W. Schnelle, A. Yaresko, Yu. Grin. On the electronic and structural properties of aluminum diboride Al<sub>0.9</sub>B<sub>2</sub>, *J. Solid State Chem.* 2004, 177, 389–394, <https://doi.org/10.1016/j.jssc.2002.12.001>

- [25] L. Akselrud, Yu. Grin, *WinCSD* (version 4), Software Package for Crystallographic Calculations, Max-Planck-Institut für Chemische Physik fester Stoffe, Dresden (Germany) 2014. See also: L. Akselrud, Yu. Grin, *WinCSD: software package for crystallographic calculations* (Version 4), *J. Appl. Crystallogr.* 47 (2014) 803–805, <https://doi.org/10.1107/S1600576714001058>
- [26] R. H. Blessing, An empirical correction for absorption anisotropy, *Acta Crystallogr. A* 51 (1995) 33–38, <https://doi.org/10.1107/S0108767394005726>
- [27] A. Altomare, M. C. Burla, M. Camalli, G. L. Casciarano, C. Giacovazzo, A. Guagliardi, A. G. G. Moliterni, G. Polidori, R. Spagna, *SIR97: a new tool for crystal structure determination and refinement*, *J. Appl. Crystallogr.* 32 (1999) 115–119, <https://doi.org/10.1107/S0021889898007717>
- [28] G. M. Sheldrick, *Shelxt - integrated space-group and crystal-structure determination*, *Acta Crystallogr. A* 71 (2015) 3–8, <https://doi.org/10.1107/S2053273314026370>.
- [29] L. J. Farrugia, *WinGX suite for small-molecule single-crystal crystallography* (*WinGX*, Version 1.64.05), *J. Appl. Crystallogr.* 32 (1999) 837–838, <https://doi.org/10.1107/S0021889899006020>
- [30] K. Brandenburg, *Diamond* (version 2.1c), Crystal and Molecular Structure Visualization, Crystal Impact - H. Putz & K. Brandenburg GbR, Bonn (Germany) 1999.
- [31] K. Schwarz, P. Blaha, G. K. H. Madsen, Electronic structure calculations of solids using the WIEN2k package for material sciences, *Comput. Phys. Commun.* 147 (2002) 71–76, [https://doi.org/10.1016/S0010-4655\(02\)00206-0](https://doi.org/10.1016/S0010-4655(02)00206-0)
- [32] P. Blaha, K. Schwarz, G. K. H. Madsen, D. Kvasnicka, J. Luitz J., *WIEN2K: An Augmented Plane Wave + Local Orbitals Program for Calculating Crystal Properties*, TU Wien (Austria) (2001).
- [33] Blaha, P.; Schwarz, K.; Tran, F.; Laskowski, R.; Madsen, G. K. H.; Marks, L. D. WIEN2k: An APW+lo program for calculating the properties of solids. *J. Chem. Phys.* **2020**, *152*, 074101. <https://doi.org/10.1063/1.5143061>
- [34] J. P. Perdew, K. Burke, M. Ernzerhof, Generalized gradient approximation made simple, *Phys. Rev. Lett.* 77 (1996) 3865–3868, <https://doi.org/10.1103/PhysRevLett.77.3865>
- [35] F. Tran, P. Blaha, K. Schwarz, P. Novák, Hybrid exchange-correlation energy functionals for strongly correlated electrons: applications to transition-metal monoxides, *Phys. Rev. B* 74 (2006) 155108, <https://doi.org/10.1103/PhysRevB.74.155108>
- [36] R. A. Susilo, X. Rocquefelte, J. M. Cadogan, E. Bruyer, W. Lafargue-Dit-Hauret, W. D. Hutchison, M. Avdeev, D. H. Ryan, T. Namiki, S. J. Campbell, Magnetic structures of  $R_2Fe_2Si_2C$  intermetallic compounds: Evolution to  $Er_2Fe_2Si_2C$  and  $Tm_2Fe_2Si_2C$ , *Phys. Rev. B* 99 (2019) 184426, <https://doi.org/10.1103/PhysRevB.99.184426>
- [37] X. Gonze, C. Lee, Dynamical matrices, Born effective charges, dielectric permittivity tensors, and interatomic force constants from density-functional perturbation theory, *Phys. Rev. B* 55 (1997) 10355–10368, <https://doi.org/10.1103/PhysRevB.55.10355>
- [38] A. I. Liechtenstein, V. I. Anisimov, J. Zaanen, Density-functional theory and strong interactions: orbital ordering in Mott-Hubbard insulators, *Phys. Rev. B* 52 (1995) R5467–R5470, <https://doi.org/10.1103/PhysRevB.52.R5467>
- [39] H. T. Stokes, D. M. Hatch, FINDSYM: program for identifying the space-group symmetry of a crystal, *J. Appl. Crystallogr.* 38 (2005) 237–238, <https://doi.org/10.1103/PhysRevB.52.R5467>

- [40] C. W. Glass, A. R. Oganov, N. Hansen, USPEX – evolutionary crystal structure prediction, *Comput. Phys. Commun.* 175 (2016) (2006) 713–720, <https://doi.org/10.1016/j.cpc.2006.07.020>
- [41] G. Kresse, J. Hafner, Ab initio molecular dynamics for liquid metals, *Phys. Rev. B* 47 (1993) 558e561, <https://doi.org/10.1103/PhysRevB.47.558>
- [42] G. Kresse, J. Hafner, Norm-conserving and ultrasoft pseudopotentials for first row and transition elements, *J. Phys. Condens. Matter* 6(1994) 8245–8257, DOI 10.1088/0953-8984/6/40/015
- [43] S. Dudarev, G. Botton, S. Savrasov, C. Humphreys, A. Sutton, Electron-energy-loss spectra and the structural stability of nickel oxide: an LSDA+U study, *Phys. Rev. B* 57(1998) 1505–1509, <https://doi.org/10.1103/PhysRevB.57.1505>
- [44] G. Kresse, J. Furthmüller, Efficient iterative schemes for ab initio total-energy calculations using a plane-wave basis set, *Phys. Rev. B* 54 (1996) 11169–11186, <https://doi.org/10.1103/PhysRevB.54.11169>
- [45] H. J. Monkhorst, J. D. Pack, Special points for Brillouin-zone integrations, *Phys. Rev. B* 13 (1976) 5188–5192, <https://doi.org/10.1103/PhysRevB.13.5188>
- [46] V. Babizhetskyy, A. Simon, K. Hiebl. Single crystal investigation and physical properties of the binary compound CeB<sub>4</sub>. *Z. Naturforsch.* 62b (2007) 896 – 900, <https://doi.org/10.1515/znb-2007-0704>
- [47] P. Pykkö, M. Atsumi, Molecular single-bond covalent radii for elements 1–118, *Chem. Eur J.* 15 (2009) 186–197, <https://doi.org/10.1002/chem.200800987>
- [48] G. A. Bain, J. F. Berry, Diamagnetic Corrections and Pascal’s Constants, *J. Chem. Educ.* 85 (2008) 532–536, <https://doi.org/10.1021/ed085p532>
- [49] R. K. Kremer, Rare Earth Magnetism – Condensed Matter, in: Rare Earth Chemistry, R. Pöttgen, Th. Jüstel, C. A. Strassert (Eds.), de Gruyter STEM, 2020, <https://doi.org/10.1515/9783110654929>
- [50] K. R. Lea, J. M. Leask, W. P. Wolf, The Raising of Angular Momentum Degeneracy of f-Electron Terms by Cubic Crystal Fields, *J. Phys. Chem. Solids* 23 (1962) 1381–1405. [https://doi.org/10.1016/0022-3697\(62\)90192-0](https://doi.org/10.1016/0022-3697(62)90192-0)
- [51] See for example: N. Grewe, F. Steglich, Heavy Fermions, in Handbook on the Physics and Chemistry of Rare Earths, (K. A. Gschneidner Jr., L. Eyring (Eds.), North-Holland, Amsterdam, Vol. 14 (1991) p. 343.